Friction **12**(6): 1165–1175 (2024)
https://doi.org/10.1007/s40544-023-0791-1
ISSN 2223-7690
CN 10-1237/TH
RESEARCH ARTICLE

A new method to solve the Reynolds equation including mass-conserving cavitation by physics informed neural networks (PINNs) with both soft and hard constraints

Yinhu XI[1,*], **Jinhui DENG**[1], **Yiling LI**[2]

[1] *School of Mechanical Engineering, Anhui University of Science and Technology, Huainan 232001, China*

[2] *Ericsson AB, Datalinjen 3, Linköping 58330, Sweden*

Received: 13 April 2023 / Revised: 22 May 2023 / Accepted: 21 June 2023

Abstract: In this work, a new method to solve the Reynolds equation including mass-conserving cavitation by using the physics informed neural networks (PINNs) is proposed. The complementarity relationship between the pressure and the void fraction is used. There are several difficulties in problem solving, and the solutions are provided. Firstly, the difficulty for considering the pressure inequality constraint by PINNs is solved by transferring it into one equality constraint without introducing error. While the void fraction inequality constraint is considered by using the hard constraint with the max-min function. Secondly, to avoid the fluctuation of the boundary value problems, the hard constraint method is also utilized to apply the boundary pressure values and the corresponding functions are provided. Lastly, for avoiding the trivial solution the limitation for the mean value of the void fraction is applied. The results are validated against existing data, and both the incompressible and compressible lubricant are considered. Good agreement can be found for both the domain and domain boundaries.

Keywords: Reynolds equation, mass-conserving cavitation, physics informed neural networks, hard constraints, trivial solution

1 Introduction

Cavitation can often be found for diverging gaps when the lubrication liquid pressure drops to the value lower than the atmospheric saturation one, and both a vapor phase and a liquid phase will be involved. The lubrication film may be ruptured for the cavitation zones, and numerous studies can be found due to the importance. For the cavitation research there are still some open questions, such as the effects of the micro-jet and the shockwave caused by the cavitation on the pitting [1]. In this work we focus on the cavitation in lubrication, and extensive papers on this topic for both numerical and experimental ways can be found, and the reader is referred to the reviews of Dowson et al. [2], Braun et al. [3], Geike [4], and Kamat et al. [5]

For analyzing the lubrication problems, the Reynolds equation has been widely used, but the effects of cavitation are not considered in it. In order to analyze the film pressure behaviors with the cavitation effects, attempts have been made by many researchers and different cavitation models have been developed [6]. Among of them, the mass-conserving cavitation model was firstly proposed by Jakobsson [7]. Later, Elrod and Adams [8] proposed a cavitation model, two variables, i.e., the fluid pressure p and the mass fraction θ, were employed to describe the fluid behaviors, and a switch function is required to change the character as per the cavitated index. Recently, a similar but different

* Corresponding author: Yinhu XI, E-mail: easonxiyinhu@gmail.com

model was developed by Giacopini et al. [9], in which the fluid pressure p and the void fraction r were utilized to form the complementarity relationship, and the two variables were valid for both lubricated and cavitation regions. Later, Bertocchi et al. [10] incorporated the compressible, piezo-viscous and shear thinning behaviors into the cavitation model. Almost at the same time, Almqvist et al. also adjusted the complementarity variables by using the constant bulk modulus, and the compressibility can be considered [11].

Moreover, it is hard to obtain the analytical solution of the Reynolds equation with or without considering the effects of the cavitation. Therefore, numerical methods are often employed by researchers, such as the finite difference method (FDM), the finite element method (FEM), and the finite volume method (FVM) [12–16].

As one branch of artificial neural network (ANN), the physics informed neural networks (PINNs) method was proposed by Raissi et al. in 2019 [17]. Different from the traditional ANN, it is unnecessary to employ a large number of data to train the neural network, but by using the known physics information itself to find the solution. It will bring unique advantage for engineering practical problems, because sometimes it is very hard to obtain enough data for the training of the traditional ANN, and therefore the PINNs method has been applied in many fields, such as for the fatigue prognosis of mechanical systems [18], the medical image analysis [19], the heat transfer problem [20], the fracture mechanics [21], and the magnetic modeling [22].

In order to solve the Reynolds equation by using the PINNs method, some reports have also been proposed recently. For example, the pioneering work of Almqvist, he firstly employed the methodology of PINNs to solve the 1D Reynolds equation [23]. Zhao et al. [24] and Li et al. [25] utilized the PINNs method to analyze the pressure results for the 2D Reynolds equation. The cavitation effect is not taken into account in the aforementioned works. Recently, Rom [26] focused on the Reynolds equation with consideration of the effects of the cavitation by using the PINNs method. The classical Elrod model was employed to model the cavitation. It can be seen that the results agree well with the results obtained from the existing numerical models in most domain. Moreover, he pointed out that some obvious error can be found for the boundary pressure values.

In this work, the mass-conserving complementarity formulation proposed by Giacopini et al. [9] was employed to study the cavitation. One of the novelties in this work is that the complementarity relationship between p and r is utilized directly to form one loss function, and the nonnegative constrains of p is employed as one more loss function. The constraint for r is considered by using the hard constraint. Moreover, in the aforementioned works, similar to the partial differential equation (PDE) loss functions, the boundary conditions are also applied by using the loss functions, i.e., the soft constrains, that can be seen as one source of the large error for the results on the boundaries. In order to overcome this shortcoming, the network architecture was adjusted in the current work, and the boundary conditions can be satisfied naturally and exactly by using the hard constraints [27].

2 The mathematic model and the PINNs framework

2.1 The mathematic model

As presented in Eq. (1) [9], the 1D Reynolds equation for compressible fluids can be expressed as

$$\frac{\partial}{\partial x}\left(\frac{\rho h^3}{6\mu}\frac{\partial p}{\partial x}\right)-2\frac{\partial(\rho h)}{\partial t}-U\frac{\partial(\rho h)}{\partial x}=0 \tag{1}$$

in which ρ is the density, h is the film thickness, μ is the lubrication viscosity, p is the pressure, and U is the surface velocity.

In order to describe the complementarity relationship for considering the cavitation effects, the void fraction r is introduced and defined as given in Eq. (2) [9].

$$r=1-\frac{\rho}{\rho_p} \tag{2}$$

where ρ_p denotes the lubrication density at the given pressure p. By substituting Eq. (2) into Eq. (1) the Reynolds equation can be expressed in Eq. (3):

$$\frac{\partial}{\partial x}\left(\frac{h^3}{6\mu}\frac{\partial p}{\partial x}\right)-U\frac{\partial h}{\partial x}+U\frac{\partial(rh)}{\partial x}-2\frac{\partial h}{\partial t}+2\frac{\partial(rh)}{\partial t}=0 \tag{3}$$

The complementarity relationship of the two variables p and r will be used [9] and is described in Eq. (4):

$$\begin{cases} p \geq 0 \\ 0 \leq r \leq 1 \\ p \cdot r = 0 \end{cases} \tag{4}$$

It can be seen that both p and r should be non-negative values, while their product for any position should be zero. In this work, we will use PINNs method to find the solution of Eqs. (3) and (4). More detail of the mathematic model can be found in the work of Giacopini et al. [9].

2.2 The PINNs framework

The PINNs architecture for 1D Reynolds equation with cavitation is presented in Fig. 1, and the coordinate x is used as the input layer. For 2D Reynolds equation, the coordinate y can also be added in the similar way for the input layer. The number of hidden layer as shown here is 3, and for each hidden layer a fixed number of neurons can be specified. There are two approximate solutions, i.e., $\hat{p}$ and $\hat{r}$, are used in the output layer. Here, $\hat{p}$ and $\hat{r}$ should satisfy the PDE as described in Eq. (3). Due to the complementarity relationship between p and r as given in Eq. (4), two inequality constraints and one equality constraint are needed. Moreover, the pressure values on the boundaries are also applied in the boundary conditions.

However, it should be noted that it is difficult to satisfy the inequality constraints directly and accurately for PINNs [27]. Therefore, the following adjustments are employed in this work. For the inequality constrain for p, as presented in Eq. (5), we transfer it into one equality constrain with no additional assumptions. In other words, there is no error for the transformation from the inequality constrain to the equality constrain.

$$\mu_1(1-\text{sign}(p))\cdot\text{abs}(p)=0 \tag{5}$$

Specially, if $p \geq 0$, $(1-\text{sign}(p))$ should be zero and $(1-\text{sign}(p))\cdot\text{abs}(p)=0$. If $p<0$, $(1-\text{sign}(p))$ should be two, and a positive value of $(1-\text{sign}(p))\cdot\text{abs}(p)$ will be output into the loss function, and μ_1 is the corresponding hyper-parameter for the loss function. Moreover, for the equality constrain as shown in Eq. (4), we also introduce a hyper-parameter, and it can be expressed in Eq. (6):

$$\mu_2\text{abs}(p\cdot r)=0 \tag{6}$$

We can also use the similar way for r, while in this work we choose to use one hard constraint to consider about r.

Besides, as proved in the works of Zhao et al. and Rom [24, 26], if the pressure values on the boundaries are applied by using the loss function, i.e., the soft constrain method, obvious fluctuation can be found on the boundaries. For example, in the work of Zhao et al. [24], more than 10% error can be found. While

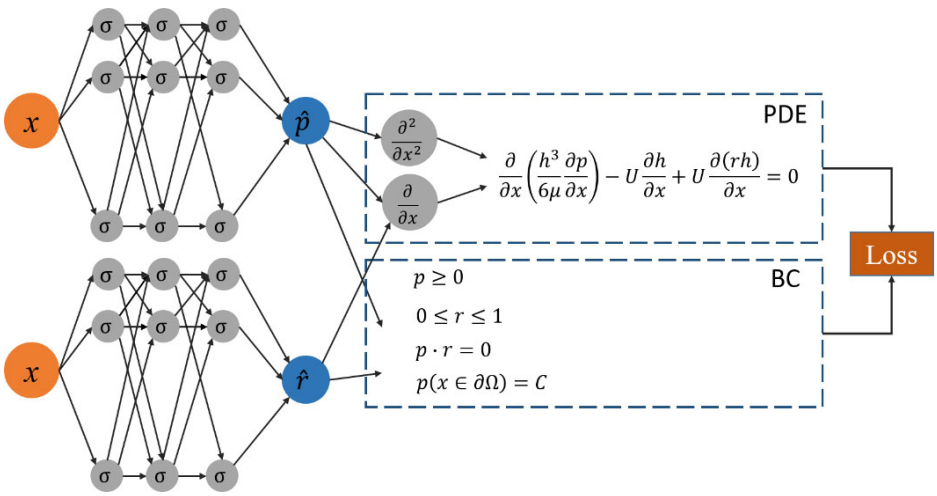

Fig. 1 PINNs architecture for the 1D Reynolds equation with cavitation.

in the work of Rom [26], only little fluctuation can be found. Therefore, it is not so promising to guarantee the boundary condition values by using the soft constrain method. In order to solve this issue, the hard constrain method will be employed [27], and the PINNs architecture with the hard constrain is described in Fig. 2. In the current work, we choose to consider about the conditions with Dirichlet boundary conditions, and for conducting the hard constrain method, we need to construct one function to satisfy the boundary conditions, and the form can be given in Eq. (7):

$$\hat{p} = g(x) + l(x)N_1(x) \tag{7}$$

in which $g(x)$ denotes the pressure values on the boundaries and $l(x)$ is a function to satisfy the corresponding conditions:

$$\begin{cases} l(x) = 0, & x \in \partial\Omega \\ l(x) > 0, & x \in \Omega - \partial\Omega \end{cases} \tag{8}$$

in which $\partial\Omega$ denotes the boundaries and Ω denotes the computational domain.

For the other output r, as we mentioned before, the value of r should be between 0 and 1, and we also employ one function to satisfy it and can be given in Eq. (8):

$$\hat{r} = \max(0, \min(N_2(x), 1)) \tag{9}$$

It should be noted that, from the mathematic view, the all zero results of p and all one results of r can satisfy the Eqs. (3) and (4), but they are obvious not our solution. Actually, the PINNs method may fail when it does find the minimum but the trivial solution. In order to avoid the trivial solution, some different methods can be applied. For example, if we know the pressure results at some points we can use them as the anchors in our training. Or if we know the total load we can also use it as one loss function.

In the current work, similar to the work presented by Lu et al. [27], we choose to limit the mean value of r, and the equation is given in Eq. (10):

$$\text{mean}(r) \le 0.9 \tag{10}$$

The main advantage of the current way is that it is unnecessary to know the accurate values of p or r beforehand for any point inside the domain. As we mentioned before for PINNs method it is very hard to satisfy the inequality constrain directly and accurately, and similar to the method used in Eq. (5), we also form one equation to describe it and can be given in Eq. (11):

$$\mu_3(1 - \text{sign}(0.9 - \text{mean}(r))) \cdot \text{abs}(\text{mean}(r)) = 0 \tag{11}$$

where μ_3 is the hyper-parameter, and it should be clarified that the introduction of the mean value of r is only employed as the constrain to avoid the trivial solution. Actually, the limitation of the mean value can be adjusted, and we found 0.8 or 0.95 can also be used. Besides, in order to guarantee the satisfaction of the three derived equality constraints as shown in Fig. 2 the large values of μ_1, μ_2, and μ_3 are used, and in the following calculation all the three hyper-parameters are fixed at 1,000.

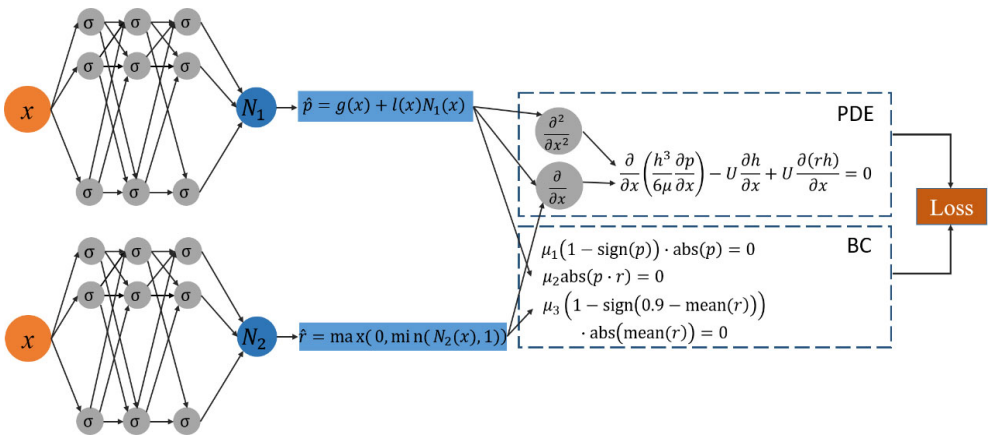

Fig. 2 PINNs architecture with hard constrains for the 1D Reynolds equation with cavitation.

It should be noted that Rom conducted the pioneering work for solving the Reynolds equation with consideration of the mass-conserving cavitation [26]. The differences between the work of Rom and the current work are presented in the following:

(1) For the work of Rom [26], two variables, i.e., the fluid pressure p and the mass fraction $\theta = \rho / \rho_{c,}$ were used, in which ρ_c denotes the density of the lubricant at the cavitation pressure, and the complementarity relationship $p(1-\theta)=0$ was employed. In our work, the void fraction variable $r = 1-\rho/\rho_0$ was used, in which ρ_0 denotes the fluid density in the full film region and is supposed to be constant [9]. The complementarity relationship $pr = 0$ was used.

(2) In the work of Rom [26], in order to use the complementarity relationship $p(1-\theta)=0$, a switch function is required to eliminate the pressure terms in the cavitation zones. Therefore, threshold values of p and θ are required to format the loss functions for the PDE term and the boundary condition terms. In our work it is unnecessary to use the switch function for using the complementarity relationship $pr=0$, and we can format the loss function for the PDE term directly.

(3) For the boundary condition terms, we try to transfer the inequality constraints to the equality ones without introducing errors, and hard constraints for the boundary conditions are employed in the current work.

(4) For the work of Rom [26], the fluid was assumed as incompressible one. In our work both the incompressible one and the compressible one are considered.

3 Results and discussion

3.1 1D condition with incompressible lubricant

Firstly, the bearing of sinusoidal profiles with pure sliding motion was calculated [28]. Here, the viscosity of the lubricant μ is fixed at 0.015 Pa·s, the film height h (mm) can be expressed in Eq. (12):

$$h = 0.02 + 0.005\sin(2\pi\frac{x}{a}+\frac{\pi}{2}) \tag{12}$$

in which the length a is 125 mm. The surface velocity U is 4 m/s, and the cavitation pressure P_c is fixed at zero. Two cases of the boundary pressure values are considered. For case A, both the inlet pressure P_0 and the outlet pressure P_1 are set as 0. For case B, both of them are set as 1 MPa.

For both cases A and B, $l(x) = x(1-x)$. While the definitions of $g(x)$ are different, and for case A, $g(x)=0$, while for case B, $g(x)=1$.

Therefore, the functions for applying the boundary values by using the hard constraint method are presented in Eqs. (13) and (14) for cases A and B, respectively. The results can be found in Fig. 3.

$$\hat{p} = x(1-x)N_1 \tag{13}$$

$$\hat{p} = 1 + x(x-1)N_1 \tag{14}$$

The number of training points is fixed at 2,000, and 3 hidden layers with 64 neurons for each one are utilized. The Adam optimizer is employed to train the networks for 20,000 epochs with the 0.001 learning rate, and then the L-BFGS will be utilized until the

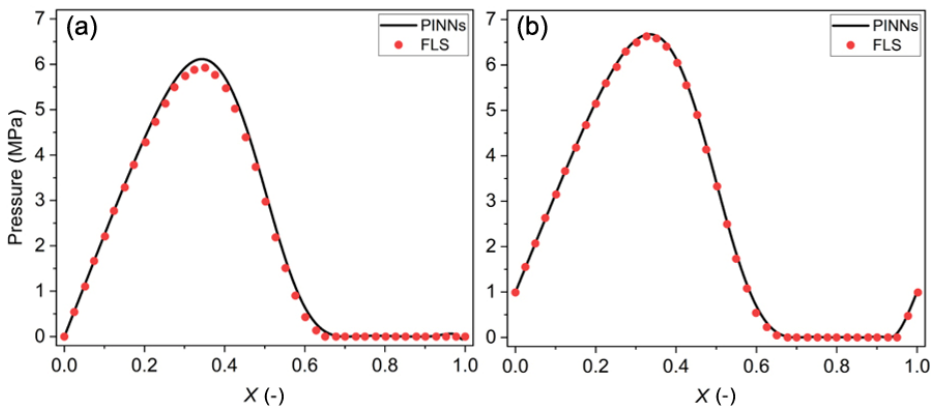

Fig. 3 Comparison of the results from the PINNs method versus the ones from the full linear system (FLS) method [28] for (a) Case A and (b) Case B.

loss is converged. The training works are conducted by using a Nvidia T1000 GPU, and the training time is around 80 s for each case.

The results are validated against to the results derived from the full linear system (FLS) [28], and the results obtained from the current PINNs method agree well with the ones of FLS. The largest error is less than 3% for case A. For case B the results from the two methods are almost the same. Moreover, it should be noted that the values for both case A and case B are guaranteed accurately.

3.2 1D condition with compressible lubricant

In this part, we will consider the condition proposed by Bertocchi et al. [10], in which the compressibility of the lubricant is taken into account. The Dowson and Higginson model was used to describe the compressibility of the lubricant, and can be given in Eq. (15):

$$\frac{\rho}{\rho_c}=\frac{C_1+C_2(P-P_c)}{C_1+(P-P_c)} \tag{15}$$

where the constants C_1 and C_2 are set as $2.22e^9$ and 1.66, respectively [29]. The film height (μm) is given by

$$h=H_0+A\frac{(x-a/2)^2}{(a/2)^2} \tag{16}$$

in which both H_0 and A are 4 μm, and the bearing length a is 76.2 mm. The surface velocity U is 4.57 m/s, the viscosity μ is 0.039 Pa·s and the cavitation pressure P_c is fixed at zero.

Different inlet and outlet pressure values are applied, the inlet one P_0 is set as 0.336414 MPa and outlet one P_1 is zero. To achieve this, the function for the hard constraint method presented in Eq. (17) is used.

$$\hat{P}=(P_1-P_0)x+P_0+x(1-x)N_1 \tag{17}$$

For the inlet boundary, by substituting $x=0$, the value of $\hat{P}$ is P_0. Similarly, if $x=1$, the value of $\hat{P}$ is P_1. Therefore, Eq. (16) can satisfy the requirement. The network parameters are the same as the ones in Section 3.1.

As can be seen Fig. 4, the current results are comparing to the ones of Bertocchi [10], and good agreement can be found.

However, due to the maximum pressure is much larger than the boundary value, and it is difficult to show the effects of the pressured inlet. In other words, we cannot verify the boundary value of P_0 easily. In order to emphasize the effects of the nonzero value of P_0, we choose to use the parameters used in the work of Sahlin et al. [29], in which most parameters are the same as the ones used by Bertocchi, but the values of H_0 and A are selected as 25.4 μm.

As can be seen in Fig. 5, the current results agree well with the ones from Sahlin et al. [29], and the maximum error is less than 1.5%. Moreover, it is easy to find that the current hard constrained PINNs method can capture the nonzero inlet boundary pressure accurately.

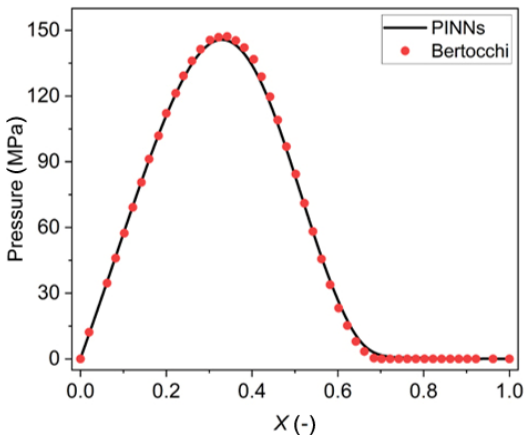

Fig. 4 Comparison of the PINNs results versus the ones of Bertocchi [10].

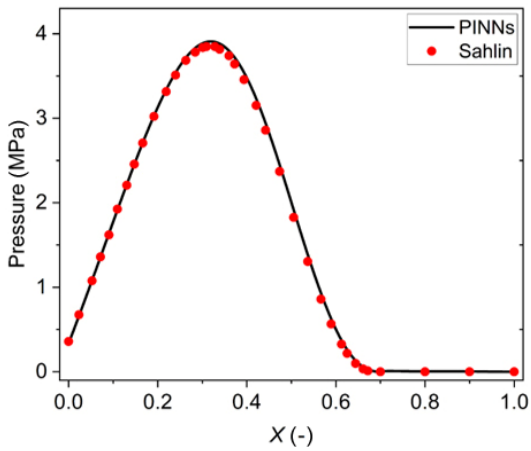

Fig. 5 Comparison of the PINNs results versus the ones of Sahlin [29].

3.3 Journal bearings with incompressible lubricant

The film pressure examples for journal bearings are conducted in this section. Firstly, the journal bearing with the incompressible lubricant condition is considered, and the parameters used by Rom are selected [26]. Specially, the bearing diameter d is $80/\pi$, the bearing width w is 20 mm, the clearance c is 17.5 μm, the eccentricity ratio e_r is 0.8, the lubricant viscosity μ is 0.014 Pa·s, the surface velocity U is 0.2 m/s, and the boundary pressure values P_b are fixed at 0.1 MPa.

The number of training points is 20,000, and the other network parameters are the same with the ones used in Section 3.1. The training time is around 1,200 s. Moreover, to improve the results on the boundaries, the hard constrain method is employed again. Here, the function as given by Eq. (18) is utilized.

$$\hat{P} = P_b + x(\pi d - x)y(w - y)N_1 \tag{18}$$

The film pressure results can be found in Fig. 6, and in order to validate our results against the ones of Rom, the pressure results along $y = 0.01$ m are extracted and are presented in Fig. 7. It can be seen that the current results agree well with the results of Rom.

As we mentioned before, a great advantage by using the hard constraint method is that the boundary values can be guaranteed mathematically. As can be seen in Fig. 8, the fluctuation of the boundary pressure values is reduced significantly by using the hard constraint method.

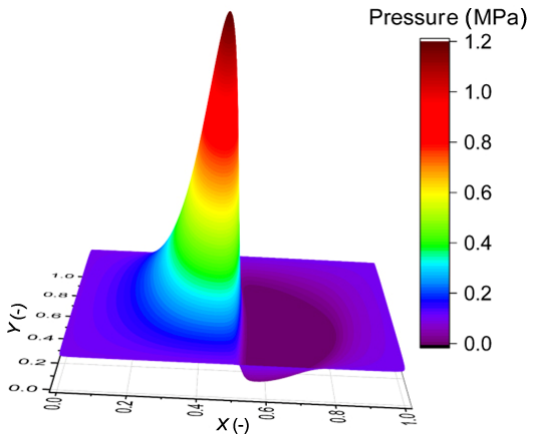

Fig. 6 Film pressure results for the journal bearing with incompressible lubricant.

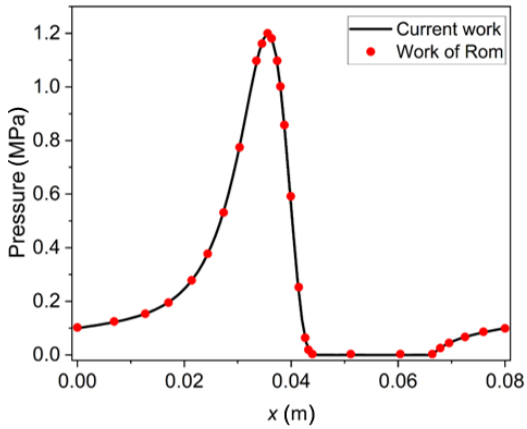

Fig. 7 Comparison of the film pressure results of the mid-plane from the PINNs method versus the ones of Rom [26].

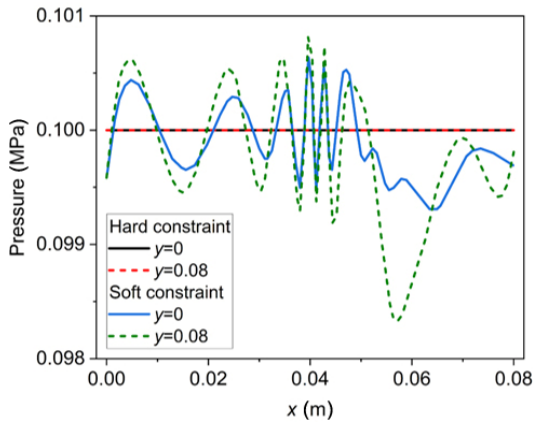

Fig. 8 Comparison of the boundary pressure results from the PINNs method with hard constraints versus the one with soft constraints [26].

3.4 Journal bearings with compressible lubricant

For the journal bearing with consideration of the lubricant compressibility, we plan to compare our results with the ones of Miraskari [28]. The dimensionless pressure results P_{non} were employed by them, as presented in Eq. (19), and therefore the parameters required for describing the journal bearing are the eccentricity ratio $e_r = 0.8$ and the bearing length to diameter ratio $l/d = 1$. Moreover, to describe the lubricant compressibility, the constant bulk modulus model is used and the bulk modulus β is set as 2×10^9 Pa.

$$P_{non} = \frac{4c^2}{\mu\Omega d^2}P \tag{19}$$

The network parameters are the same with the

ones used in Section 3.3. As can be seen in Fig. 9, the maximum P_{non} is around 71, and the pressure results along the middle plane of the Y axis are comparing to the ones of Miraskari [28]. Good agreement can be found as can be seen in Fig. 10.

In the above-mentioned examples, the cavitation pressures are all set as zero. However, it should be noted that for the work of Rom [26] the absolute pressure was employed due to the ambient pressure was also set as 0.1 MPa, while in the works of Bertocchi et al., Sahlin et al., and Miraskari et al. [10, 28, 29] the gauge pressure was used because the ambient pressures were zero. It should be noted that different cavitation pressures were reported in some experimental works [30], and for the absolute way the cavitation pressures for journal bearings are varied from 29.2 kPa to 95.7 kPa (absolute) [31]. In order to consider about the non-zero cavitation pressure, the complementarity relationship of p and r provided in Eq. (4) is described in Eq. (20):

$$\begin{cases} p - p_c \geq 0 \\ 0 \leq r \leq 1 \\ (p - p_c) \cdot r = 0 \end{cases} \tag{20}$$

The first two equality constraints used in the PINNs architecture are revised in Eqs. (21) and (22).

$$\mu_1 (1 - \text{sign}(p - p_c)) \cdot \text{abs}(p - p_c) = 0 \tag{21}$$

$$\mu_2 \text{abs}((p - p_c) \cdot r) = 0 \tag{22}$$

The current results are validated against the ones obtained from the method of Almqvist [11], and both the inlet and outlet pressures are set as 0.1 MPa (absolute). Two cavitation pressure values, i.e., 0.03 MPa and 0.09 MPa (absolute), are considered. The viscosity of the lubricant μ is 0.02 Pa·s, and the film height h (mm) is given in Eq. (23):

$$h = 0.02 + 0.01 \sin\left(2\pi \frac{x}{a} + \frac{\pi}{2}\right) \tag{23}$$

in which the length a is 100 mm. The surface velocity U is 1 m/s, and the bulk modulus β is set as 2×10^9 Pa. The results are provided in Fig. 11, and it can be seen that the current results agree well with the ones of Almqvist. Moreover, we can find that the current PINNs method can capture the cavitation pressure values well through enlarged details.

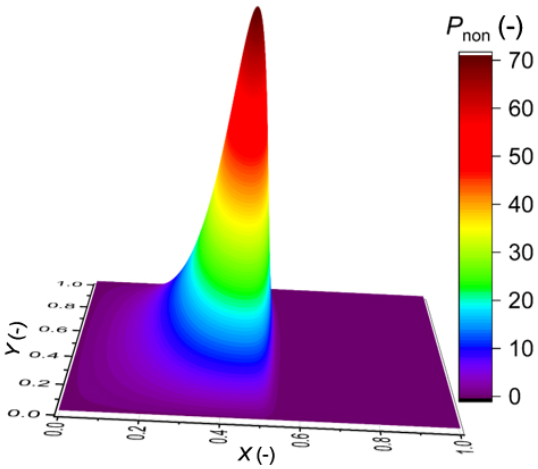

Fig. 9 Film pressure results for the journal bearing with compressible lubricant.

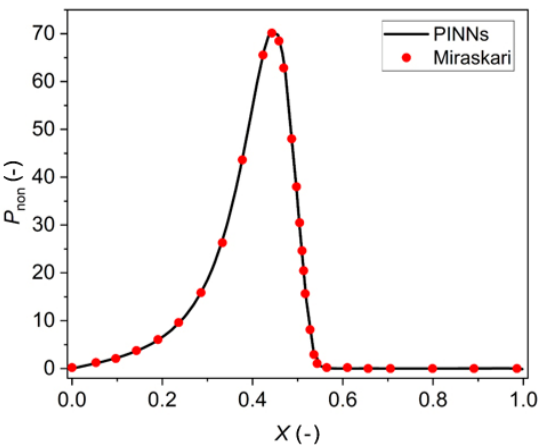

Fig. 10 Comparison of the pressure results of the mid-plane from the PINNs method versus the ones from the work of Miraskari [28].

3.5 Limitations

The PINNs method has demonstrated the great potential to solve the Reynolds equation with or without considering about the cavitation. However, it also should be noted some limitations when using it.

1) It is difficult to consider the discontinuity film height conditions, but they can also be found in practice, such as for pocket bearings [4, 6] and the textured journal bearings [25]. Due to the non-differentiable nature at the discontinuity points, we cannot employ the PINNs method to obtain the solutions directly.

2) The training time is normally much longer than some sophisticated methods. For the current study,

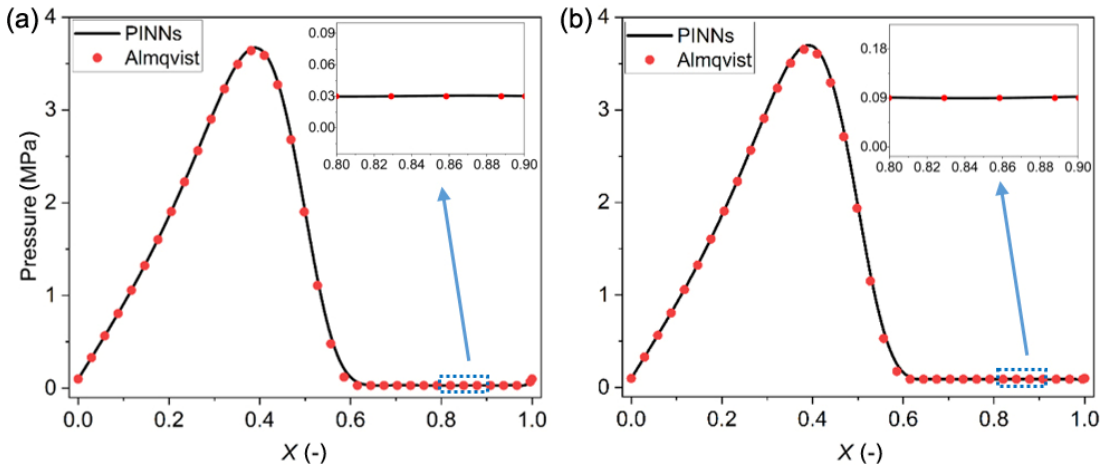

Fig. 11 Comparison of the pressure results from the PINNs method versus the ones from the method of Almqvist [11] for (a) $p_c = 0.03$ MPa (absolute) and (b) $p_c = 0.09$ MPa (absolute).

we use a T1000 GPU to conduct the calculation. For the 1D Reynolds equation, about 80 s are required, while for the 2D one, about 1,200 s are needed. We believe by using one more advanced GPU we can reduce the time to some extent, but it is still much longer than the existing numerical methods, such as the FDM.

4 Conclusions

In this work, the Reynolds equation with considering of the mass-conserving cavitation is solved by using the PINNs method. The inequality constraint for pressure is transferred into the equality one without introducing any error, and the one for void fraction is guaranteed by using the hard constraint method. In order to reduce the fluctuation and inaccuracy of the soft constraint method on the boundaries, we also employed the hard constraint method to construct the neural networks. Both the incompressible and the compressible lubricant conditions are considered, by comparing with the existing data from several researchers for both 1D and 2D conditions, and the accuracy of the current PINNs method has been validated. Moreover, due to the employment of the hard constraint method to describe the pressure values on the boundaries, the accuracy of the boundary pressure values is improved significantly. Besides, the limitations of the current method are also discussed. We believe the PINNs method can be used for other forms of lubrication, and in our next study we will try to use it to solve the EHL problem.

Acknowledgements

The authors would like to thank the funding from Anhui University of Science and Technology (No. 2022yjrc15), the Key Project of National Natural Science Foundation of China (Nos. U21A20125 and U21A20122), the Key Research and Development Projects of Anhui Province (No. 2022a05020043), and the National Natural Science Foundation of China (Nos. 51805410 and 51804007).

Declaration of competing interest

The authors have no competing interests to declare that are relevant to the content of this article.

References

[1] Dular M, Požar T, Zevnik J, Petkovšek R. High speed observation of damage created by a collapse of a single cavitation bubble. *Wear* **418–419**: 13–23 (2019)

[2] Dowson D, Taylor C M. Cavitation in bearings. *Annu Rev Fluid Mech* **11**: 35–65 (1979)

[3] Braun M J, Hannon W M. Cavitation formation and modelling for fluid film bearings: A review. *Proc Inst Mech Eng Part J* **224**(9): 839–863 (2010)

[4] Geike T. Review on the bubble dynamics based cavitation dynamics for the negative squeeze motion in lubricated contacts. *Front Mech Eng* **6**: 33 (2020)

[5] Kamat H, Kini C R, Shenoy S B. Effect of cavitation and temperature on fluid film bearing using CFD and FSI technique: A review. *Arch Computat Methods Eng* **30**(3): 1623–1636 (2023)

[6] Wang W, He Y Y, Zhao J, Mao J Y, Hu Y T, Luo J B. Optimization of groove texture profile to improve hydrodynamic lubrication performance: Theory and experiments. *Friction* **8**(1): 83–94 (2020)

[7] Jakobsson B, Floberg L. The finite journal bearing, considering vaporization (Das Gleitlager von endlicher Breite mit Verdampfung). *Trans Chalmers University of Technology* **1957**: 190 (1957)

[8] Elrod H G, Adams M L. A computer program for cavitation and starvation problems. *Cavitat Relat Phenom Lubr* **1**: 37–13 (1975)

[9] Giacopini M, Fowell M T, Dini D, Strozzi A. A mass-conserving complementarity formulation to study lubricant films in the presence of cavitation. *J Tribol* **132**(4): 1 (2010)

[10] Bertocchi L, Dini D, Giacopini M, Fowell M T, Baldini A. Fluid film lubrication in the presence of cavitation: A mass-conserving two-dimensional formulation for compressible, piezoviscous and non-Newtonian fluids. *Tribol Int* **67**: 61–71 (2013)

[11] Almqvist A, Fabricius J, Larsson R, Wall P. A new approach for studying cavitation in lubrication. *J Tribol* **136**(1): 011706 (2014)

[12] Silva A, Lenzi V, Cavaleiro A, Carvalho S, Marques L. FELINE: Finite element solver for hydrodynamic lubrication problems using the inexact Newton method. *Comput Phys Commun* **279**: 108440 (2022)

[13] Geng Y, Chen W. Multiscale method of modelling surface texture with mass-conserving cavitation model. *Tribol Int* **173**: 107663 (2022)

[14] Gropper D, Wang L, Harvey T J. Hydrodynamic lubrication of textured surfaces: A review of modeling techniques and key findings. *Tribol Int* **94**: 509–529 (2016)

[15] Han Y X, Meng Q G, de Boer G. Two-scale homogenization of hydrodynamic lubrication in a mechanical seal with isotropic roughness based on the Elrod cavitation algorithm. *Proc Inst Mech Eng Part J* **236**(3): 359–385 (2022)

[16] Ardah S, Profito F J, Dini D. An integrated finite volume framework for thermal elasto-hydrodynamic lubrication. *Tribol Int* **177**: 107935 (2023)

[17] Raissi M, Perdikaris P, Karniadakis G E. Physics-informed neural networks: A deep learning framework for solving forward and inverse problems involving nonlinear partial differential equations. *J Comput Phys* **378**: 686–707 (2019)

[18] Yucesan Y A, Viana F A C. A hybrid physics-informed neural network for main bearing fatigue prognosis under grease quality variation. *Mech Syst Signal Process* **171**: 108875 (2022)

[19] van Herten R L M, Chiribiri A, Breeuwer M, Veta M, Scannell C M. Physics-informed neural networks for myocardial perfusion MRI quantification. *Med Image Anal* **78**: 102399 (2022)

[20] Cai S Z, Wang Z C, Wang S F, Perdikaris P, Karniadakis G E. Physics-informed neural networks for heat transfer problems. *J Heat Transf* **143**(6): 060801 (2021)

[21] Zheng B, Li T C, Qi H J, Gao L G, Liu X Q, Yuan L. Physics-informed machine learning model for computational fracture of quasi-brittle materials without labelled data. *Int J Mech Sci* **223**: 107282 (2022)

[22] Kovacs A, Exl L, Kornell A, Fischbacher J, Hovorka M, Gusenbauer M, Breth L, Oezelt H, Praetorius D, Suess D, *et al*. Magnetostatics and micromagnetics with physics informed neural networks. *J Magn Magn Mater* **548**: 168951 (2022)

[23] Almqvist A. Fundamentals of physics-informed neural networks applied to solve the Reynolds boundary value problem. *Lubricants* **9**(8): 82 (2021)

[24] Zhao Y, Guo L, Wong P P L. Application of physics-informed neural network in the analysis of hydrodynamic lubrication. *Friction* **11**(7): 1253–1264 (2023)

[25] Li L L, Li Y Z, Du Q W, Liu T Y, Xie Y H. ReF-nets: Physics-informed neural network for Reynolds equation of gas bearing. *Comput Meth Appl Mech Eng* **391**: 114524 (2022)

[26] Rom M. Physics-informed neural networks for the Reynolds equation with cavitation modeling. *Tribol Int* **179**: 108141 (2023)

[27] Lu L, Pestourie R, Yao W J, Wang Z C, Verdugo F, Johnson S G. Physics-informed neural networks with hard constraints for inverse design. *SIAM J Sci Comput* **43**(6): B1105–B1132 (2021)

[28] Miraskari M, Hemmati F, Jalali A, Alqaradawi M Y, Gadala M S. A robust modification to the universal cavitation algorithm in journal bearings. *J Tribol* **139**(3): 031703 (2017)

[29] Sahlin F, Almqvist A, Larsson R, Glavatskih S. A cavitation algorithm for arbitrary lubricant compressibility. *Tribol Int* **40**(8): 1294–1300 (2007)

[30] Manser B, Belaidi I, Hamrani A, Khelladi S, Bakir F. Texture shape effects on hydrodynamic journal bearing performances using mass-conserving numerical approach. *Tribol Mater Surf Interfaces* **14**(1): 33–50 (2020)

[31] Shen C, Khonsari M M. On the magnitude of cavitation pressure of steady-state lubrication. *Tribol Lett* **51**(1): 153–160 (2013)

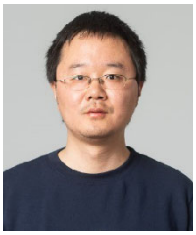

Yinhu XI. He received his bachelor and master degrees in mechanical engineering from Hefei University of Technology, China, in 2008 and 2011, and he received his Ph.D. degree in mechanical engineering from Xi'an Jiaotong University, China, in 2017. He is now an associate professor in Anhui University of Science and Technology, China. His research interest is focused on numerical simulation in tribology.